J Solid State Electrochem (2008) 12:1003–1009
DOI 10.1007/s10008-007-0465-3

ORIGINAL PAPER

Nanostructured NiO for electrochemical capacitors: synthesis and electrochemical properties

Teressa Nathan · A. Aziz · A. F. Noor · S. R. S. Prabaharan

Received: 16 August 2007 / Revised: 26 October 2007 / Accepted: 29 October 2007 / Published online: 30 November 2007

Abstract A single phase nanostructured nickel oxide (NiO) crystalline product was synthesized via a simple solvothermal synthesis protocol by using nitrate–citrate precursor having $Ni(NO_3)_2$ as starting material. The thermal decomposition of the as-formed gel precursor leading to the formation of crystalline NiO was monitored by TG analysis under ambient conditions. The as-prepared product was subjected to thermal treatment at 400 °C for 1 h in air, exhibited a single phase cubic structure as confirmed by XRD and the nanostructure of the product was characterized by FE-SEM and HR-TEM/SAED analysis. It is thus confirmed that the particle size of the product was found to be within 7–15 nm range. The rate-dependent cyclic voltammetry reveals the pseudocapacitive behavior of the product when employed as working electrode in a three-electrode electrochemical cell containing 1 M KOH aqueous electrolyte with platinum (pt) and saturated calomel electrode (SCE) as counter and reference electrodes, respectively, yielding a capacitance of ~200 F g^{-1}.

Keywords Nickel oxide · Soft-chemistry · Nanostructured materials · Electrochemical capacitors · Pseudocapacitor

Contribution to ICMAT 2007, Symposium K: Nanostructured and bulk materials for electrochemical power sources, July 1-6, 2007, Singapore

T. Nathan · A. Aziz · A. F. Noor
School of Materials and Mineral Resources Engineering,
Universiti Sains Malaysia,
Nibong Tebel, Malaysia

S. R. S. Prabaharan (✉)
School of Electrical and Electronics Engineering,
Faculty of Engineering and Computer Science,
The Nottingham University Malaysia Campus,
Jalan Broga, Selangor 43500, Malaysia
e-mail: prabaharan.sahaya@nottingham.edu.my

Present address:
T. Nathan
School of Electrical and Electronics Engineering,
Faculty of Engineering and Computer Science,
The Nottingham University Malaysia Campus,
Jalan Broga, Selangor 43500, Malaysia

Introduction

In electrochemical capacitors (EC), the energy stored is either capacitive or pseudocapacitive (a faradic battery-like reaction) in nature. The capacitive or nonfaradaic process is based on charge separation at the electrode/solution interface, whereas the pseudocapacitive process consists of faradaic redox reactions, which occur within the bulk of active electrode materials [1]. Varieties of electrode-active materials being investigated are carbons [2], conducting polymers [3, 4], and transition metal oxides [5–19]. Hydrous RuO_2 is known to exhibit outstanding properties among the many transition-metal oxide materials investigated as pseudocapacitor material. An amorphous phase of $RuO_2\ xH_2O$ formed by the sol–gel method at low temperatures shows a specific capacitance as high as 720 F g^{-1} in an acidic electrolyte [5]. However, the high cost of these materials limits its commercial use. Hence, a great deal of effort has been focused on searching for alternative transition metal oxides as electrode materials, for instance nickel oxide [6–15] cobalt oxide [16] and manganese oxide [17–19], which are inexpensive and exhibit pseudocapacitive behavior similar to that of hydrous RuO_2.

Nickel oxide possesses both Faradic charge transfer reaction (battery-like) and the nondiffusional charge reaction (capacitor-like) characteristics together with high bulk

electronic conductivity. These properties are particularly important for EC applications [20–22]. Liu et al. [23] have also synthesized a porous nickel oxide films with the sol–gel process, but the films could only provide a specific capacitance of 50–64 F g^{-1}. These studies ensure the limited electrochemical utilization of nickel oxide materials although it possesses high theoretical specific capacitance of 2584 F g^{-1} within 0.5 V [24]. This high specific capacitance value makes nickel oxide being regarded as a potential positive electrode material for electrochemical capacitors (ECs). However, due to various preparation conditions, the available nonstoichiometry in NiO (either $Ni_{1-x}O$ or NiO_{1-x}) limits the achievable specific capacitance ranged from 50 to 300 Fg^{-1}. In general, it is expected that the electrochemical redox reaction in NiO facilitates the transfer of two electrons (Ni^{2+} to Ni^{4+}) delivering a large reversible specific discharge capacity.

To circumvent these potential limitations, asymmetric hybrid ECs were also proposed and developed by Beliakov et al. [25, 26], in which a cell couple was formed by a carbon double-layer material as negative electrode and an oxide pseudocapacitive material as a positive electrode. This asymmetric electrode configuration facilitates the higher operating voltage (1.2 V) even in aqueous electrolyte whose theoretical decomposing voltage is considered to be at 1.23 V. Nevertheless, NiOOH/carbon asymmetric EC reportedly showed a wide operating voltage window of 1.75 V in KOH aqueous electrolyte and a high-energy density of about 8–10 Wh kg^{-1}. It is likely that this impressive value could be achieved due to charge storage in the above asymmetric EC utilized both surface and bulk redox activity. As a consequence, this diminishes the power density of 80–100 W kg^{-1} compared to in pure double-layer electrode because of the bulk ionic diffusion limitations and large redox reaction time constant in the above asymmetric device. To overcome the above problem in asymmetric ECs, it must be ensured that a positive electrode should have a high rate capability keeping the maximum active material utilization. One of the promising ways to increase the rate capability is to creating nanoscale properties within the materials itself. Tailoring nickel oxide in its nanoscale could bring new impetus to various applications offering great opportunities for researchers to challenge its unique physico-chemical properties particularly in energy storage device.

In the recent years, nanoscale electrode materials have attracted a great deal of interests since the nanoscale electrodes show better rate capabilities than conventional electrodes composed of the same materials. The surface area of nanoscale electrode is much larger, leading to the effective current density smaller than conventional electrode at the same current density during charge and discharge. Due to reduced particle size within nanoscale, the following advantages are realized: (1) the required diffusion length in the active materials, (2) reduce the effective specific current density in the rapid charge–discharge process, (3) realizing high cycle performance even at rapid charge–discharge process, and (4) increases the electronic conductivity of the electrodes. Hither to, nickel oxide has been obtained through different techniques, for instance thermal decomposition involving liquid phase processes [27], coprecipitation [13, 28], sol–gel method [23] and electrochemical oxidation [29, 30]. Recently, Zhang et al reported that NiO nanoparticles of ~9 nm could be synthesized via thermal decomposition of NiC_2O_4 nanofibres [13]. All these processes require stringent preparation procedure in a way or other to prepare bulk quantities of nanoscale nickel oxide.

Accordingly, this paper reports on our success in producing nanoscale bulk powders of phase pure NiO via a simple solution-based synthesis protocol and the electrochemical redox properties were studied by using rate-dependent cyclic voltammetry.

Experimental details

Synthesis of nanoscale nickel oxide

Synthesis of nanoscale powders of nickel oxide was accomplished by means of a combined citrate–nitrate solution method via a simple solvothermal approach previously described by us [31]. In the present work, nanostructured NiO powder was synthesized via a nitrate–citrate method using $Ni(NO_3)_2$ as starting material in the presence of citric acid dissolved in methanol/acetone mixture solution at a molar ratio of 1:10. Citric acid was used as a chelating agent known to induce the molecular level mixing of the dissociated metal ionic species dissolved in the solution mixture. Acetone being one of the solvents is used as a handle which promotes non-hydrolytic condensation of nickel nitrate dissolute. This process ensures formation of clear solution at all times without forming any turbid solution. The total mixture solution thus obtained was further gently stirred at 70 °C for 1 h in ambient conditions until all the solvents were evaporated, leaving a wet gel-like substance, the so-called precursor. The as-prepared gel was subsequently heated to 350 °C which ignites the organics giving rise to intense internal exothermic reaction leading to the decomposition of various organic moieties. The product thus obtained was subjected to heat treatment (annealing) at 400, 600, and 800 °C for 1 h in air to elucidate the structural/microstructural changes within the final product. Thus, this process assisted in obtaining a well-defined nanostructure of NiO product.

Effect of citric acid: solvothermal process

The mechanism of synthesizing NiO nanoparticles with the addition of citric acid (chelating agent) can be called as 'citric-acid-based solvothermal method'. Complexation is a popular method of modifying ligands in the original precursor solution, and carboxylic acid or β-diketones are the most frequently used complexing agents, which slow down the pace of hydrolysis and condensation [16]. Citric acid is the widely being used as complexing agent for solution based solvothermal methods for preparing electrode-active transition metal oxides [31]. Citric acid (H3L) is a weak triprotic acid which dissociates in a stepwise manner in solution depending upon the solution pH; only when pH value of the solution is > 6 [35], the species L becomes the dominant one. The complexation reactions between metal ions and citric acid are also highly dependent upon the pH of the solution and cannot occur, in general, in a very strong acidic solution. However, we did not alter the pH of the total solution as the mixture solution quickly forms a clear solution (without adding ammonia water) upon slow heating the total solution while gently stirring. Considering the reaction of chelating agent, we suggest that citric acid coordinated to Ni ions in $Ni(NO_3)_2$ methanolic solution, making the nucleation complete at the early stage of the solvothermal process and inhibiting the crystal growth.

Structural and microstructural characterization

The structural and morphological properties of nickel oxide were determined by means of XRD, FE-SEM and HR-TEM techniques. To study the crystallinity, the as-prepared product was further annealed at 400, 600, and 800 °C for 1 h in air, showed cubic crystallographic phase without any residual impurities as confirmed by powder X-ray diffraction (XRD) using a Siemens Diffractometer D5000 with CuKα radiation (λ=1.5418 Å). The FE-SEM (Zeiss -LEO supra 35 VP equipped with 3rd Generation Gemini field emission column) was used to observe the morphology and the degree of agglomeration. The HR-TEM analysis was also carried out using a Philips CM 12(s) TEM. The linear sweep cyclic voltammetry technique was applied employing an electrochemical workstation (Autolab PGSTAT 302) to investigate the pseudocapactive properties using a standard three electrode cell having platinum (pt) and SCE as counter and reference electrode respectively. The potential window used was within 0.4 V vs SCE at different scan rates.

Electrode preparation and electrochemical characterization

The composite nickel oxide electrode was prepared using a standard procedure by mixing NiO/polyvinylidene fluoride (PVdF)/acetylene black in 80:10:10 weight ratios. The composite electrodes were made by dispersing the above mixture in n-methyl pyrrolidone (NMP) to form a slurry. Carbon black was added to increase the electrode conductivity of NiO powders. The thick slurry was then coated on a 4 cm^2 stainless steel mesh expanded mesh (EXMET, USA). This was then rolled into thin sheets of around 1 μm thick, and cut into circular electrodes of 3.14 cm^2 area and pressed onto SS expanded grid mesh current collector under a pressure of 100 kg/cm^2. The pressed pellets were then heated at 100 °C for 24 h to ensure complete dryness.

An open-beaker three-electrode cell, comprising active material electrode (composite electrode cut into a pre-determined size) as working electrode, saturated calomel electrode as the reference electrode and platinum foil as the counter electrode was set-up. Aqueous 1 M of KOH was utilized as electrolyte solution. This experiment was conducted to study the redox behavior of the synthesized material. The working electrode was degassed in vacuum in the electrolyte solution before cyclic voltammetry (CV) test to increase the wettability between the electrode and the electrolyte. It has been proven that the wetted pores increase the ionic motion, which in turn maximizes the energy storing capacity during polarization [32].

Results and discussion

TG analysis

The phase formation of nickel oxide was studied using TG analysis. Figure 1 shows the TG thermogram obtained from the dried gel precursor mass which was recovered before the precursor spontaneously being thermally decomposed during the synthesis process described elsewhere in the present work. As seen from Fig. 1, the weight change occurs in different temperature regimes: two prominent weight losses are evident, the first one being 12% from RT up to 110 °C with stepwise features related to the eva-

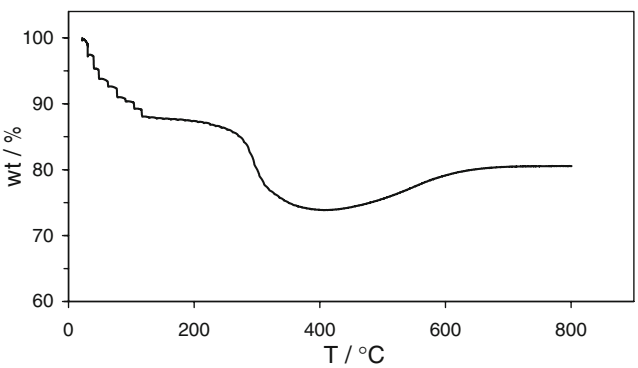

Fig. 1 TG Analysis of nickel nitrate precursor showing the phase formation reaction

poration of free water and residual methanol and the second weight loss occurs at ~220 °C with ~ 22% accompanied by a heavy exothermal feature which could be related to the decomposition of citrate groups and NO_3 ions, and the condensation of Ni–OH surface groups. The phase formation of the final product (NiO) was complete after the exothermic reaction that occurred at an onset temperature of ~ 300 °C where there was a huge weight loss occurred followed by the decomposition of nitrate leading to NiO phase. Interestingly, it is found that the weight loss due to decomposition stops at about 400 °C followed by a significant weight gain occurs up to a temperature of ~600 °C. It is likely that the latter weight gain reaction could be the result of formation of NiO/Ni nanocomposite which in turn further oxidized (in air/O_2) due to extended heating beyond 400 °C. The redundant formation of Ni is attributed to the oxygen deficiency experienced during the thermal decomposition of the organic moieties at about 350 °C which incited the NiO to reach its metallic state probably due to lack of oxygen partial pressure in the vicinity of the decomposition. Beyond 650 °C the weight remains constant indicating the completion of the oxidation process.

Phase analysis

The diffractograms of nanosized NiO powders showed well crystalline product even at temperature as low as 400 °C is shown in Fig. 2. Figure 2a exhibits the characteristics broadness in the diffractograms revealing the nanostructure nature of the powder sample. The peaks were indexed using least square refinement analysis and were found to be in accordance with the standard spectrum of NiO (JCPDS, card no. 47–1049). The width of the bragg reflections is considerably broadened, indicating a small domain size of the crystallites. The broadenings diminish with the increase of heat treatment temperatures, suggesting the growth of the

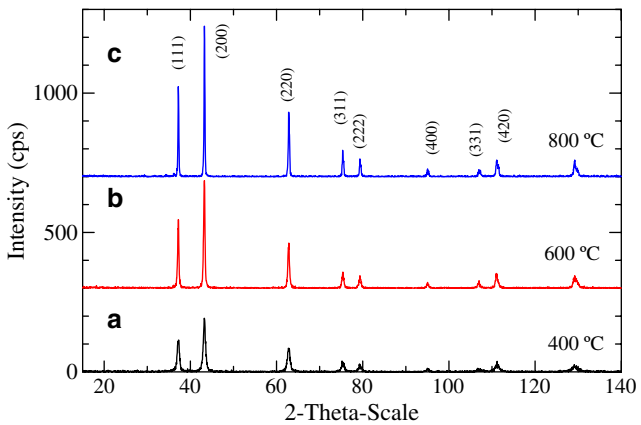

Fig. 2 Indexed X-ray diffractograms of NiO at different heat treatment temperature

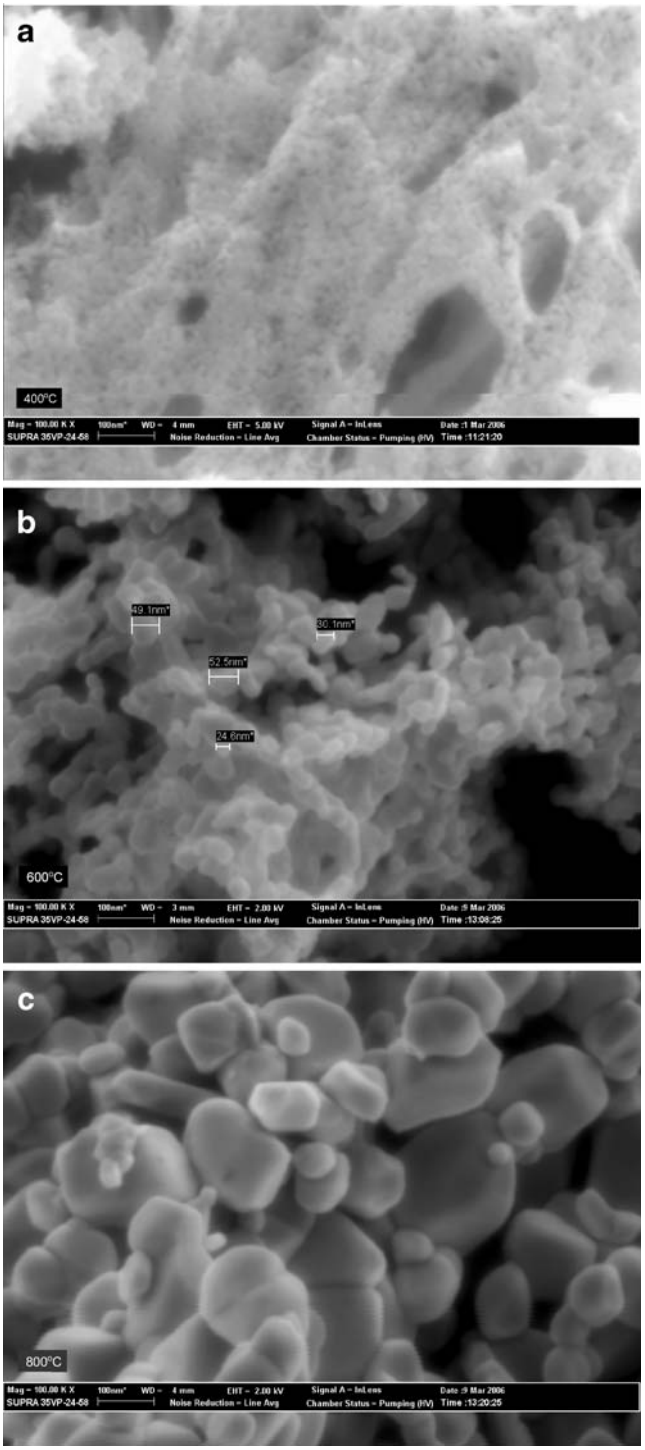

Fig. 3 FE-SEM pictures of NiO heated at **a** 400 °C, **b** 600 °C, and **c** 800 °C in air for 1 h

NiO crystallites. It can be seen that all the particles are in nanometer scale and grow slowly with the increase of heat treatment temperature. Figure 2b and c exhibit the sharp peaks due to the effect of heat treatment at 600 and 800 °C (1 h/air). All the diffraction peaks were indexed to pure cubic NiO phase with cubic lattice parameter $a(b=c)=$ 4.174 Å (space group: Fm3 m), which is in agreement with

the reported value (JCPDS 47–1049). As the heat treatment temperature increases, the crystal structure of NiO becomes well refined as revealed from the sharp diffraction peaks demonstrating the increased crystallinity of the sample.

The crystallite domain size calculation was performed for the major diffraction peak (200) using the Scherrer's formula,

$$D = \frac{0.89\lambda}{B\cos\theta} \quad (1)$$

where λ, is the wavelength of X-ray (1.5418 Å) for CuKα_1 radiation, B, full width at half maximum, FWHM of prominent intensity peak (usually the 100% relative intensity peak will be used), θ, peak position. The estimated grain size using Scherrer's formula was found to be about ~13 nm which is in good agreement with FE-SEM/TEM findings as discussed further. The expected shape factor k of the average crystallite in the present case is considered to be 0.89 due to the presence of spherical grains of the final product. It is seen that the crystallite size calculated from TEM micrographs is smaller than the calculated one using Scherrer's equation, due to the obvious fact that all the errors were not eliminated while calculating the crystallite size. Since powder samples were used to obtain the XRD pattern, the broadening due to mechanical strain and instrument errors were ignored too.

FE-SEM/HR-TEM analysis

The nanostructure morphology of the final product (both as-prepared and calcined) was confirmed by FE-SEM and HR-TEM analysis. FE-SEM images are shown in Fig. 3a–c for samples heated at different temperatures for 1 h in air. As exhibited in Fig. 3a, the porous morphology is evident with particles sizes within the range, 7–15 nm. The particles are uniform in size with spherical grains which are well-connected yet provide porous structure which is much required for device applications, for instance supercapacitors. As the heat treatment temperature increases, the particles tend to grow as expected, for instance at 600 and 800 °C, the size of the grains grown in the ranges, 25–50 nm and 100–150 nm, respectively. Nevertheless, at 800 °C, the shape of the grains prominently differed exhibiting bigger grains and a non-uniform grain distribution is evident. The TEM micrographs along with the SAED patterns are shown in Fig. 4 for the heated product (400 °C/1 h). It reveals the formation of uniform nanosized spherical grains with primary particles within the range 7–15 nm (average size). SAED image confirms the well-oriented crystallographic structure with diffraction rings characteristic of NiO lattice planes as shown in Fig. 4 (inset). Some high resolution (HRTEM) images show lattice fringes exhibiting the cubic order (not shown).

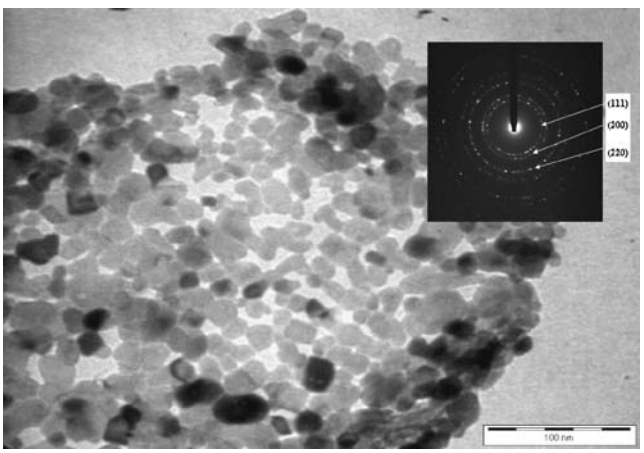

Fig. 4 TEM picture of NiO heated at 400 °C (1 h/air; *inset*: bight field SAED pattern of the NiO heated at 400°C/1 h in air)

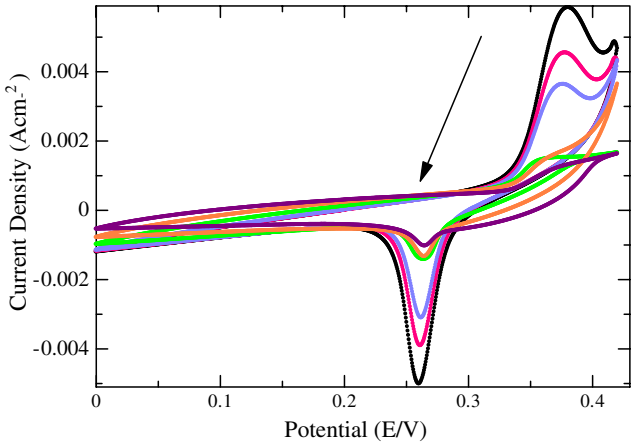

Fig. 5 Scan rate dependent cyclic voltammetry of nanostructured NiO against SCE reference electrode. *Arrow* indicate decreasing scan rate (100, 70, 50, 20, 10, and 5 mV/s)

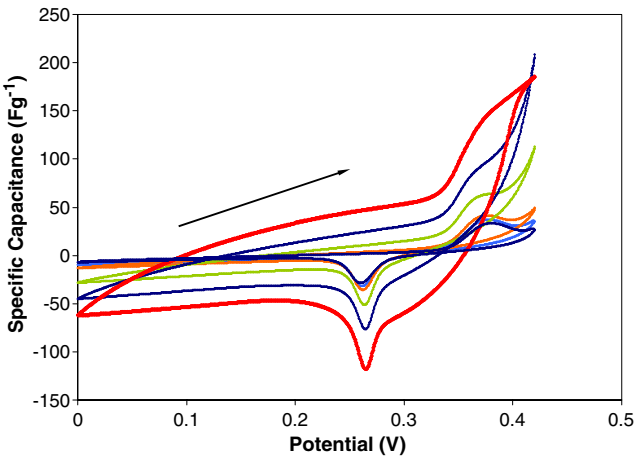

Fig. 6 Specific Capacitance versus Potential plot of nanostructured NiO against SCE reference electrode. *Arrow* indicate decreasing scan rate (100, 70, 50, 20, 10, and 5 mV/s)

Electrochemical studies

Cyclic voltammetry was employed to determine the electrochemical properties of the synthesized NiO nanostructured powder in 1 M of KOH solution. Nickel oxide annealed at 400 °C was chosen for this study. Figure 5 shows the rate dependent cyclic voltammetry (CV) of composite NiO against saturated calomel electrode (SCE). The electrode potential was scanned between 0.0 and 0.5 V vs SCE in both anodic and cathodic directions and the current responses were measured. The redox peaks during anodic and cathodic scan at different scan rates confirm the redox behavior of the synthesized product. The redox features corresponding to anodic and cathodic peaks appear at ~0.38 and 0.26 V vs SCE, respectively, at 5 mV s^{-1} up to 100 mV s^{-1}. During the anodic scan, the peak occurs at 0.38 V indicative of oxidation process while reduction takes place at 0.26 V during the cathodic scan. The appearance of anodic and cathodic peaks corresponding to the $Ni(OH)_2$/NiOOH redox reaction in the CV is according to the following electrochemical reaction:

$$NiO + OH \rightarrow NiOOH + e^- \quad (2)$$

For the extent of specific adsorption of potential can be described as the oxidation and reduction of metal ions on the oxide surface, it has been determined that these surface redox reactions may contribute to the measured capacitance over a certain potential range. Equation 2 describes the oxidation reaction of Ni^{2+} (NiO) to Ni^{3+} (NiOOH). It is believed that NiO in contact with an alkaline solution tends to change to nickel hydroxide at the surface [33, 34] forming a surface layer onto NiO probably within several angstroms [33] of the nickel oxide. It is believed that the proportion of nickel hydroxide formed would be proportional to the area of nickel oxide exposed to the solution.

The capacitance (C) of an electrode may be defined by

$$C = \frac{dq}{dv} = \frac{i}{dv/dt} \quad (3)$$

where q is the charge on the electrode, v is its potential, and I the instantaneous current. For systems involving faradaic, an operational definition of an effective capacitance requires the specification of a practical range of potential in which charge-transfer reactions are reversible and do not cause deterioration of the electrode during cycling. Therefore, the capacitance C may be reported as an average value in Eq. 3 applied to various experimental tests within the specified potential range. In contrast to the differential capacitance, C as defined by Eq. 3, the integral charge-storage capacity (q) is defined here as the total surface-charge density and calculated from the CV curves according to the following equation:

$$q = \int i \times t \quad (4)$$

where i is the instantaneous anodic current density when the potential is given and t the sampling time in seconds. Accordingly, the maximal capacitance has been calculated to be ~200 F g^{-1} (see Fig. 6). This value is superior to other similar works reported earlier. The electrochemical redox behavior of the product obtained showed clearly resolved peaks which corroborate its charge transfer reversibility and it stability against variation in scan rate. Nanostructured NiO thus obtained demonstrated excellent specific capacitance up to 200 F g^{-1} in alkaline electrolyte solution (1 M KOH) and could be used as a pseudocapacitor electrode in hybrid electrochemical capacitors. The detailed study on the performance of NiO as positive electrode in a hybrid capacitor against a mesoporous carbon will be reported elsewhere.

Conclusion

The present work describes the pseudocapacitive behavior of the nanoscale NiO product synthesized via a novel solvothermal approach at temperature as low as 400 °C. The nanostructured morphology of the synthesized NiO was confirmed by FESEM, TEM, and XRD techniques with particle sizes as small as 7–15 nm range. Cyclic voltammograms showed clearly resolved peaks which corroborate with its charge transfer reversibility and its stability against variation in scan rates. The presence of macroscopic properties such as particle sizes in nanometer scale, large exposed surface areas, and high surface energy help enlarge the contact area, electron tunneling length thus improving the electrode conductivity and enhance the electrochemical rate kinetics as demonstrated in this work. The specific capacitance up to 200 F g^{-1} in alkaline electrolyte solution (1 M KOH) confirms that nanostructured electrode materials could certainly outperform compared to the conventional electrode materials.

References

1. Conway BE (1999) Electrochemical supercapacitors: scientific fundamentals and technological applications. Kluwer, New York, p 13
2. Frackowiak E, Beguin F (2001) Carbon 39:937
3. Villers D, Jobin D, Soucy C, Cossement D, Chahine R, Breau L, Belanger D (2002) J Electrochem Soc 149:A167
4. Fusalba F, El Mehdi N, Breau L, Belanger D (2000) Chem Mater 12:2581

5. Zheng JP, Cygan PJ, Zow TR (1995) J Electrochem Soc 142:2699
6. Liu KC, Anderson MA (1996) J Electrochem Soc 143:124
7. Srinivasan V, Weidner JW (1997) J Electrochem Soc 144:L210
8. Nam KW, Kim KB (2002) J Electrochem Soc 149:A346
9. Nam KW, Yoon WS, Kim KB (2002) Electrochim Acta 47:3201
10. Prasad KR, Miura N (2004) Appl Phys Lett 85:4199
11. Nam KW, Kim KB (2001) Electrochemistry (Tokyo, Japan) 69:467
12. Lee SH, Tracy CE, Pitts JR (2004) Electrochem Solid State Lett 7: A229
13. Zhang F, Zhou Y, Li H (2004) Mater Chem Phys 83:260
14. Nelson PA, Owen JR (2003) J Electrochem Soc 150:A1313
15. Ganesh V, Lakshminarayanan V (2004) Electrochim Acta 49:3561
16. Lin C, Ritter JA, Popov BN (1998) J Electrochem Soc 145:4097
17. Lee HY, Goodenough JB (1999) J Electrochem Soc 144:220
18. Pang SC, Anderson MA, Chapman TW (2000) J Electrochem Soc 147:444
19. Hu CC, Tsou TW (2002) Electrochem Commun 4:105
20. Kotz R, Carlen M (1999) Electrochim Acta 45:2483
21. Burke A (2000) J Power Sources 91:37
22. Trasati S, Kurzweil P (1994) Platinum Metal rev 38(2):46
23. Liu KC, Anderson MA (1996) J Electrochem Soc 143:124
24. Nam KW, Lee ES, Kim JH, Lee YH, Kim KB (2005) J Electrochem Soc 152:A2123
25. Beliakov AI, Brintsev AM (1997) in Proceedings of the 7th International Seminar on Double Layer Capacitors and Similar Energy Storage Devices, Florida Educational Seminars, Boca Raton, FL
26. Razoumov S, Klementov A, Litvinenko S, Beliakov A (2001) US Pat 6,222,723
27. Wang X, Song J, Gao L, Jin J, Zheng H, Zhang Z (2005) Nanotechnology 16:37
28. Srinivasan V, Weidner JW (2000) J Electrochem Soc 147:A880
29. Nam KW, Lee ES, Kim JH, Lee YH, Kim KB (2005) J Electrochem Soc 152:A2123
30. Chigane M, Ishikawa M (1998) J Chem Soc Faraday Trans 94:3665
31. Prabaharan SRS, Michael MS, Prem Kumar T, Mani A, Athinarayanasamy K, Gangadharan R (1995) J Mater Chem 5 (7):1035–1037
32. Endo M, Kim YJ, Osawa K, Ishii K, Inoue T, Nomura T, Miyashita N, Dresselhaus MS (2003) Electrochem Solid State Lett 6:A23
33. Gao M, Huang S, Dai L, Wallace G, Gao R, Wang Z (2000) Angew Chem Int Ed 39:3664
34. Hughes M, Shaffer MSP, Renouf AC, Singh C, Chen GZ, Fray DJ, Windle AH (2002) Adv Mater 14:382
35. Choy J-H, Han Y-S (1997) J Mater Chem 7:1815